Characterization of Tensile Damage for a Short Birch Fiber-reinforced Polyethylene Composite with Acoustic Emission

Alencar Bravo*[1], Lotfi Toubal[2], Demagna Koffi[3], Fouad Erchiqui[4]

[1,2,3]Laboratory of Mechanics and Eco-Materials, University of Quebec at Trois-Rivières, 3351, boul. des Forges, C.P. 500, Trois-Rivières (Québec), Canada

[4]Laboratory of Biomaterials, University of Quebec at Abitibi-Témiscamingue, 445, boul. de l'Université, Rouyn-Noranda (Quebec), Canada

[1]alencar.soares.bravo@uqtr.ca; [2]lotfi.toubal@uqtr.ca; [3]koffi@uqtr.ca; [4]fouad.erchiqui@uqat.ca

Abstract

A biocomposite was prepared using paper industry wood fibers (birch) mixed with a thermoplastic matrix of linear low-density polyethylene (LLDPE) at various fiber weights. Monotonic and load-unload tensile tests were performed at room temperature. The acoustic emission (AE) technique was used to characterize microstructural damage events leading to overall failure of the biocomposite. The behavior evolution (stress/strain) of the biocomposite appears to be correlated with the evolution of the AE cumulative energy, exhibiting four phases. The failure mechanisms in the short fiber-reinforced thermoplastic composites were identified using a neural network based on a Kohonen non-supervised self-organizing map (KSOM). Three parameters of the AE burst signals (amplitude, count and duration) were found to be very useful in classifying damage modes. As a result, a new damage mode definition is proposed based on a neural network with three parameters. The participation of each mode in the final failure was evaluated. The results indicated that fiber content plays a primary role in biocomposite failure. This finding has been further supported by scanning electron microscopy (SEM) micrographs of the fractured face.

Keywords

Acoustic Emission; Birch; Biocomposite; Damage Mechanics; Neural Network; Polyethylene

Introduction

The term, biocomposite, is employed when natural fibers are used as an environmentally friendly alternative to replace composites with traditional fibers. Biocomposites were developed in response to the recent increased need for more ecologically friendly and low-cost materials. Some advantages of natural fibers include their singular properties of low density, high specific strength, enhanced energy recovery, CO_2 neutral after burning, easy processing, bio-degradability and low cost. However, their applications are primarily limited to decorative or non-loading bearing uses. This research aims to expand our understanding of the degradation of these materials and to enhance knowledge of its uses, such as in mechanical gears. Therefore, quantitative analyses and methodologies to assess the behavior of these materials, their properties and their failure modes are extremely important.

In this work, a biocomposite material is developed using paper industry wood fibers (birch) mixed with a thermoplastic matrix of linear low-density polyethylene (LLDPE). Compared to other semi-crystalline polymers, LLDPE has the highest ductility at room temperature. Birch is a common hardwood tree that grows in cool areas with abundant precipitation, such as the province of Quebec, which contains approximately 50% of the growing stock volume of yellow birch in North America. The combination of the two materials results in a biocomposite that is easy to fabricate and consequently should be very affordable.

However, it is surprising how few studies have investigated the damage of LLDPE reinforced with birch fiber. Gu and Raj studied the properties of this type of thermoplastic matrix but used an aspen fiber and they have not studied the damage. Some studies have been conducted to obtain an enhanced interface between two naturally incompatible constituents: hydrophilic fibers and a hydrophobic matrix. Recently, Lafia-Araga tested red balau fibers using various thermal treatments at the fiber level. These researchers observed an increase in matrix/fiber adhesion, which improved the mechanical properties. The use of a coupling agent can also enhance the mechanical properties by improving the matrix/fiber interface. Nevertheless, there is still a lack of comprehensive studies on the failure processes of a thermoplastic matrix of LLDPE reinforced with short fibers (birch).

TABLE 1 LITERATURE REVIEW ON DAMAGE MODES OF COMPOSITES WITH RESPECT TO THE AMPLITUDE RANGE.

Author	Matrix	Fiber	Matrix micro-cracking	Matrix/matrix friction	Debonding	Matrix/fiber friction	Fiber breakage
El Mahi et al.	Epoxy	Flax	42-60 dB	-	60-70 dB	-	70-100 dB
Kotsikos et al.	Polyester	Glass	40-55 dB	-	55-70 dB	-	80-100 dB
Czigány	Poly-propylene	Basalt	21-30 dB	35-45 dB	45-60 dB	-	60-100 dB
Elouaer et al.	Poly-propylene	White hemp and chènevotte	40-60 dB	-	60-65 dB	65-85 dB	85-95 dB
Laksimi et al.	Poly-propylene	Glass	33-45 dB	45-58 dB	58-67 dB	67-85 dB	85-100 dB
Meraghni and Mullin	Epoxy	Glass	35-48 dB	48-60 dB	60-65 dB	65-82 dB	82-100 dB

To achieve this aim, monotonic and load-unload tensile tests were conducted to measure the mechanical properties and failure mechanism evolution caused by irreversible changes in the material due to the application of stress. Acoustic emission (AE) testing was carried out to assess damage mechanisms and their evolution in tensile-test specimens.

Mehan is first researcher to correlate failure mechanism with an acoustic signature (AS). Conventional mechanism analysis is performed by investigating histograms of cumulative hits versus amplitude. The results of amplitude discrimination in composites are available in the literature and are reviewed in Table 1.

In our case, it is important to note that some factors can alter the amplitude of a microstructural event: 1) LLDPE dampers the amplitude at very short distances and 2) fibers obtained from plants have cellular structures that are assembled through a hierarchical process in nature and therefore are not homogeneous. The consequence of these two factors is that damage classifications based on burst amplitude can be inaccurate.

One option is to use artificial neural networks to correct dubious microstructural event classifications using other burst shape information. For this purpose, the Kohonen non-supervised self-organizing map (KSOM) is used; which has a learning style that allows relationships in the input data to be maintained in the output. The working principle of an artificial neural network is based on soft-competitive learning in which adjacent neurons are weighted by a neighborhood function. Although analysis by neural networks may be useful, the results must be corroborated by external knowledge.

This paper is organized as follows. First, the material proprieties and damage level progression are analyzed using mechanical parameters such as stiffness reduction. Second, the damage is evaluated in terms of the AE energy released during various phases using the material condition and changes in shape of the stress/strain curve. Third, the degradation is analyzed in detail using a developed two-step methodology for damage mode characterization in biocomposites with neural networks. Fourth, the results of the mechanical measurements of damage and the AE are combined to verify their correlation. Finally, our conclusions are validated by fractured face scanning electron microscope (SEM) micrographs.

Materials and Experimental Testing

Materials

For this experiment, an LLDPE thermoplastic matrix (Novacor® HI-0753-H) donated by NOVA Chemicals was used with industrial short fibers (thermomechanical pulping, 35 mesh size) of yellow birch (Betula alleghaniensis). The fibers were produced by the Lignocellulosic Materials Research Centre, Trois-Rivieres (Canada) and were dried at 60°C in an air-circulated oven for 24 hours before use.

All of the specimens were prepared using a two-roll mill (Thermon C.W. Brabender, Model T-303) with a 0.6 gear ratio. Grains of LLDPE were melted on rollers at 170°C, and fiber was subsequently added according to the desired weight ratio (0, 10, 20 and 30 wt%).

Dog-bone specimens in accordance with the norm ISO 527-2 were obtained through molding processes. This norm suggests a specimen shape with a length greater than 150 mm and a width of 4 mm. The mold was maintained at a temperature of 205°C by means of a Dake press for 20 minutes under a pressure of 20 MPa.

Experimental Testing

At room temperature, monotonic and load-unload tensile tests were performed following the standards of ISO 527-4. The tests were carried out using an electromechanical testing machine, Instron model LM-U150, equipped with a 150-kN load cell (Fig. 1). During tensile testing, a 25mm extensometer was connected to the data acquisition system and fixed on the gauge length section of the specimen to record the strain evolution.

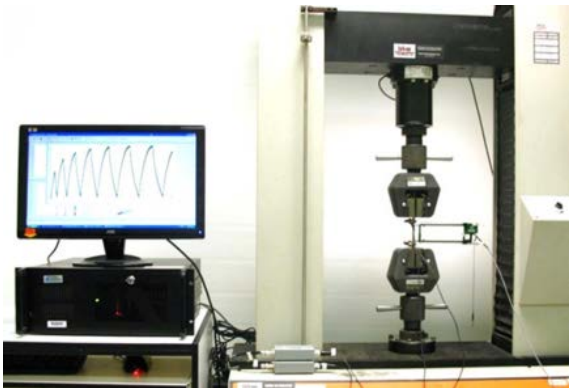

FIG. 1 TENSILE MACHINE TESTING, WITH ACOUSTIC EMISSION EQUIPMENT ON THE LEFT

AE measurements were conducted using devices provided by Physical Acoustics Corporation (PAC), equipped with two PCI cards. Two sensors (type Micro-80 PAC, wideband 100-1000 kHz) were mounted to the surface of the test specimen at a spacing of 70 mm. An acoustic threshold level set at 35 dB was used to filter background noise. A silicone adhesive gel was employed as a coupling agent between the sensors and the specimen. Before each test, the quality of the coupling was verified using a Nielsen-Hsu pencil lead break.

The quality of the measured AE data depends mainly on the choice of the waveform system timing parameters, namely, peak definition time (PDT), hit definition time (HDT) and hit lockout time (HLT). The values of the timing parameters employed are: PDT= 40 μs, HDT = 80 μs and HLT = 200 μs.

Mechanical Behavior Results

Material Properties

Fig. 2a shows the stress-strain curves recorded during monotonic tensile testing while Fig. 2b shows results for the 20 wt% sample, with the monotonic and load-unload tests superposed. The static strength properties are given in Table 2.

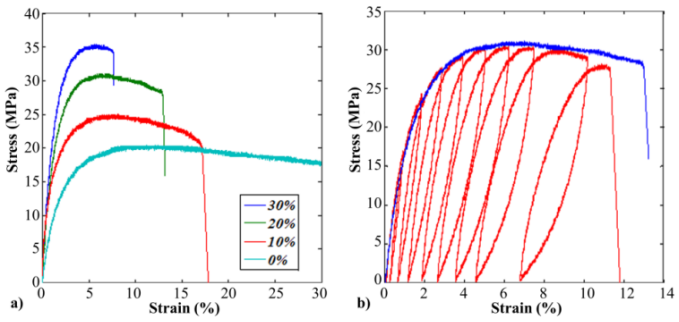

FIG. 2(a) RESULTS FROM THE TENSILE TESTS OF SPECIMENS WITH DIFFERENT FIBER WEIGHTS; (b) RESULTS FOR 20 WT% WITH THE MONOTONIC AND LOAD-UNLOAD TESTS SUPERPOSED.

The manufacturing protocol used in this work demonstrates a good reproducibility of measurements with a low standard deviation. An increase in the fiber proportion reduces the ductility of the material while increasing the Young's modulus and the ultimate strength (cf. Table 2). Compared to a pure matrix, the Young's modulus increases to 98%, 144% and 178% for biocomposites of 10 wt%, 20 wt% and 30 wt% fiber, respectively. In the same order, the ultimate strength increases to 51%, 88% and 94%.

TABLE 2 TENSILE TEST DATA: AVERAGE ULTIMATE STRENGTH AND YOUNG'S MODULUS.

Fiber (wt%)	Young's modulus		Ultimate strength		Strain failure	
	E (GPa)	STD DEV	σ (MPa)	STD DEV	ε (%)	STD DEV
0%	0.91	0.07	16.97	2.56	-	-
10%	1.81	0.11	25.62	1.44	15.46	3.60
20%	2.22	0.18	31.87	1.12	11.39	1.77
30%	2.53	0.27	33.04	1.85	7.17	2.08

These results indicate that 30 wt% approaches the optimum fiber content ratio in these biocomposites, as the maximum load improves by only 6% compared to the result for 20 wt%. This is very low compared to the improvement gained by using 20 wt% versus 10 wt% (37%). Overall, the results are interesting considering that no treatment or coupling agent was used to improve the cohesion of the fiber-matrix interface.

Property Degradation and Failure

As no standard test method exists for load/unload tests, a sufficient number of cycles was chosen to cover the different phases that describe the behavior of the biocomposite. At room temperature, load-unload longitudinal tensile tests were performed as follows: the specimen is loaded until it reaches a certain strain, then the loading is removed. Afterwards, the material is subjected to a higher strain level.

Fig. 3a displays the evolution of residual strain for different fiber weights. The axis of abscissa refers to the maximum strain obtained in each cycle before the unloading phase begins. For all samples, the occurrence of residual strain is measured at 2% of the maximum strain.

In the initial linear elastic range, the biocomposite behaves as a homogeneous material, with the fibers and matrix experiencing the same strain. Above the elastic limit, due to the difference in their Young's moduli, shear force accumulates in the matrix/fiber interface. At this point, the stress and strain in the two components are partially decoupled due to the matrix

viscoelasticity. Consequently, the matrix will be compressed and the fiber will be under tensile stress after the unloading phase.

The shear stress in the components will increase, ultimately resulting in the detachment of the fibers from the matrix. If this detachment occurs, damage is induced in the matrix, the yield limit increases and more residual strain is observed. In the case of the 10 wt% specimen, above 10% strain, we can assume that the shear limit of the interface is reached, subsequently causing fiber pullout. Due to the occasioned subsequent fiber detachment, the semi-crystalline LLDPE can reach a higher residual strain. This phenomenon is noted above 4.2% of residual strain with a continuous rate of increase of the residual strain.

The change in the elastic modulus is commonly used to document irreversible changes in the properties of materials due to the application of cyclic stresses or strains. The cumulative damage, D (mechanical damage index), is defined as:

$$D = 1 - E_i/E_o \quad (1)$$

where E_i is Young's modulus after the ith cycle and E_0 is the initial modulus.

Fig. 3b presents the evolution of damage accumulation for all specimens. The damage accumulation variable exhibited a logarithmic shape until the final failure occurred. The rapid increase in variable D in the first cycles is most likely related to the viscoelastic behavior, which temporally affects the value of Young's modulus. In this graph, the ability to bear internal damage before failure can be evaluated for each specimen. As the biocomposite fiber content decreases, more internal damage can be borne before final failure. Conversely, higher fiber content induces a more sudden brittle rupture. For 30 wt%, final breakage occurred at 65% of internal damage; for 20wt% and 10 wt%, the final breakage occurred at 69% and 73%, respectively.

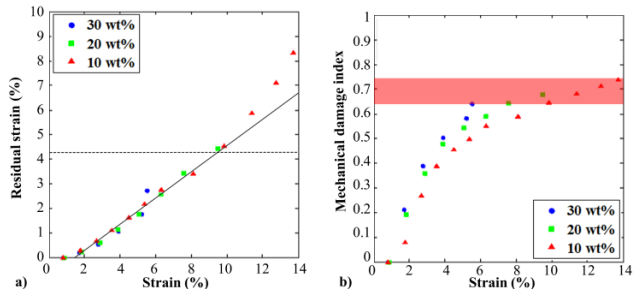

FIG. 3 (a) RESIDUAL STRAIN VERSUS STRAIN AND (b) MECHANICAL DAMAGE INDEX VERSUS STRAIN FOR 10 WT%, 20 WT% AND 30 WT% FIBER SPECIMENS.

Acoustic Emission Results

Degradation in Tensile Tests

AE tests were performed to examine the microstructural failure events contributing to the behavior of the biocomposite. The damage can be observed through the AE energy parameter. Fig. 4 shows the combination of a stress curve and the AE cumulative energy versus strain for a pure matrix and a 10 wt% fiber specimen.

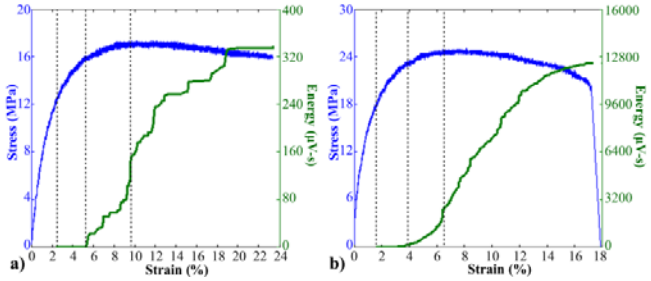

FIG. 4 TENSILE CURVES WITH CUMULATIVE AE ENERGY: (a) 0 WT% AND (b) 10 WT% FIBER.

Four phases are shown in Fig. 4. First, no acoustic activity was recorded in the first linear elastic phase (characterized by an elastic modulus E0). Second, the slope of the stress curve decreased, reflecting the beginning of viscoelastic behavior. We also denote the onset of the first AE energy measurement, with the accumulation of AE energy remaining low and constant. Third, the evolution of the AE energy curve suddenly became exponential. At this point, the stress curve is non-linear, reflecting the onset of plasticity (inelasticity). An assumption can be made that a new mechanism of damage has occurred at this point. Fourth, after the maximum load, the curve evolution of the energy changed and exhibited an almost linear form until the final breakage. Thus, the AE can be correlated to the stress/strain curve shape. These four phases could be distinguished in every specimen.

It is noted that the pure matrix has some particularities, making its phase identification more difficult. For this specimen in particular, only damage events due to matrix microcracking and matrix/matrix friction can be observed (as will be discussed later). The AE waves of these events are characterized by a lower energy. This phenomenon, together with the fact that the test was stopped before final failure (the specimen had a very high elongation, exceeding the limits of the tensile testing machine), resulted in a very low level of energy. The energy recorded at the end of the test for the pure matrix was 335 μV-s, making this curve very sensitive to variation. The total cumulative energy for the 10wt% specimen was 11500 μV-s.

Degradation in Load-unload Tests

Fig. 5 documents the evolution of cumulative energy as a function of time (for the pure matrix and the 10 wt% fiber specimen). As mentioned in the preceding section, the same phases can be observed. The acoustic activity begins with a linear elastic phase, with the detection of the first burst near 12 MPa for the pure matrix and 18 MPa for the 10 wt% specimen. A significant energy value only appears when the load increases to 15 MPa for the pure matrix and to 23 MPa for the 10 wt% specimen. Afterwards, an exponential evolution takes place up to the maximum stress. The energy curve evolution subsequently becomes linear until failure. The loads corresponding to a phase boundary were the same as in the monotonic test. The advantage of this test is its ability to assess damage evolution through mechanical indicators.

The accumulated acoustical energy curve exhibits the same four phases for each specimen. The total energy produced in the pure matrix specimen is again very low (240 μV-s) when compared to the 10 wt% specimen (39654 μV-s). The fibers are responsible for some damage modes, producing considerably more energy. In the case of the biocomposite (Fig. 5b), more energy is recorded in each cycle compared to the pure matrix (Fig. 5a).

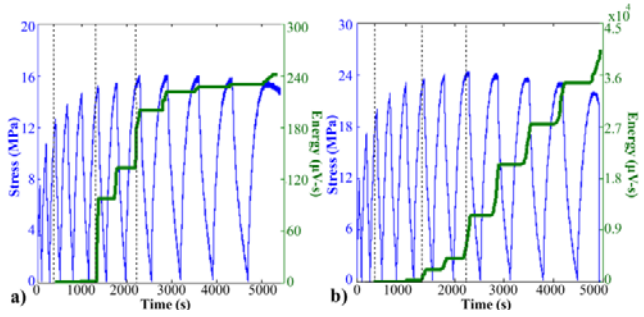

FIG. 5 ACCUMULATED AE ENERGY AND STRESS VERSUS TIME FOR LOAD-UNLOAD TESTS: (a) 0 WT% AND (b) 10 WT% FIBER..

The Kaiser and Felicity Effects

The Kaiser effect occurs in load-unload tests, when applied stress levels that were previously exerted on a material do not produce AE activity. If the Kaiser effect is present, the material is in a relatively good condition and no substantial damage was inflicted. The Felicity effect is a term used when the Kaiser effect is not observed. This effect can be described as the onset of AE events occurring before the previous maximum stress is reached.

The Felicity effect is a much less desirable damage situation because it results in a faster degradation of the material proprieties. According to Pollock, insignificant flaws tend to exhibit the Kaiser effect, while structurally significant flaws tend to exhibit the Felicity effect. Fig. 6 shows the Felicity diagram for the pure matrix and for the 10 wt% specimen.

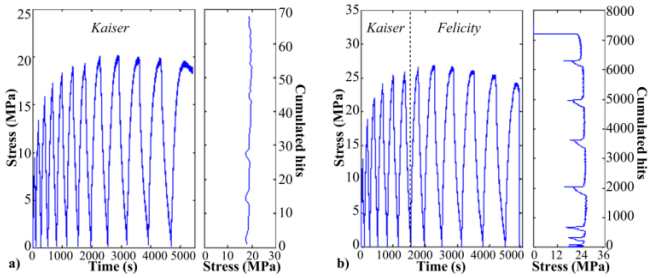

FIG. 6 STRESS VERSUS TIME AND FELICITY EFFECT DIAGRAM FOR (a) 0 WT% AND (b) 10 WT% FIBER.

The pure matrix and biocomposite behave differently regarding their Felicity effect level. While the pure LLDPE presents no Felicity effect during the test, the biocomposite has a substantial Felicity effect with a low fiber content and an increase in the total produced energy with each cycle. In the case of a 10 wt% fiber specimen, the Felicity effect begins after the sixth cycle. This point corresponds to where the third material phase begins in Fig. 5b, with an exponential increase in the energy value. Alternatively, in this phase, significant flaws are inflicted to the material, and it starts losing its mechanical stability. Therefore, in real-life biocomposite applications for a mechanically required piece, replacement must be considered at this stage. As it can be observed by comparing Fig. 4, 5 and 6, the Kaiser effect is beneficial for the pure matrix: the phase transitions not only have the same load but also the same energy level. For example, the final phase began as the total accumulated energy reached 120 μV-s in both the monotonic and the load-unload test. Conversely, the biocomposite final phase was reached at 2834 μV-s in the monotonic test and at 4152 μV-s in the load-unload test, corresponding to a difference of 46.5%.

Consequently, real-time material surveillance using the energy parameter is not recommended for certain cases, such as gear systems. In such cases, for an optimal product life cyclic design, other information might be useful, such as the load level of the material phase transition or a well-known composite AS.

Acoustic Signatures of Damage Mechanisms

Several modes of micro failure mechanisms are found in composites. For mode identification, the amplitude distribution of AE events is commonly used to describe the failure modes. The distribution of the AE

amplitude takes the form of groups, which may overlap, reflecting the failure mechanisms.

To best study failure mechanisms in biocomposites, this section is divided into two parts. First, only the failure mechanisms in the pure matrix are studied. Second, the damage modes related to the presence of fibers are discussed for the biocomposites.

Pure Matrix (0 wt% fiber): Pre-analysis of the Damage Mode Classification

Fig. 7a documents the amplitude distributions of the AE events for pure polyethylene. As previously discussed, relatively few bursts were recorded. In this context, two higher peaks are visible in the amplitude histogram at 48 dB and 40 dB, suggesting the presence of two groups of damage. This corresponds to the initiation and propagation of microcracks and matrix/matrix friction, respectively. A local valley near 45 dB indicates a borderline value.

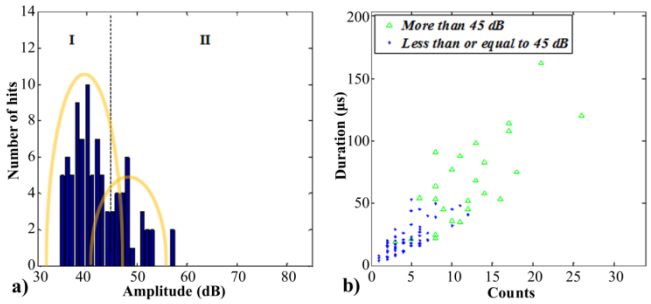

FIG. 7(a) CLASSICAL HISTOGRAM OF AMPLITUDES FOR PURE LLDPE: TWO OVERLAPPING GROUPS REPRESENTING DAMAGE MODES; (b) COUNTS VERSUS DURATION DISCRIMINATED BY AMPLITUDE.

Fig. 7b represents the shape (counts versus duration) of each burst with regard to the limit value of 45 dB. Blue spots represent bursts for which the amplitudes are between 35 dB and 45 dB, and green triangles represent amplitudes between 46 dB and 55 dB. We can attribute matrix microcracks to the blue spots, whereas the green spots have a shorter duration and a lower number of counts and can be attributed to matrix/matrix friction.

Using this classification, some bursts with approximately 5 counts at a duration of 20 µs are classified as matrix/matrix friction. However, we assume that this is a burst with matrix microcracking characteristics, so the classification may be inappropriate.

We can use amplitude discrimination with the tensile stress/strain curve. Fig. 8 illustrates burst amplitude ranges along with the tensile curve. The AE bursts between 35 dB and 45 dB are marked with an asterisk below the tensile curve. Bursts between 45 dB and 55 dB are shown as a circle above the tensile curve. The first microcrack is observed at a 12-MPa load, but the activity remains low until a load of approximately 16 MPa is reached, where a phase with several microcracking events starts. As we reach the maximum stress, the AE activity reaches its maximum. Subsequently, the AE activity rate for both modes stabilizes. This finding corroborates with the suggestion that new mechanisms start at specific phases.

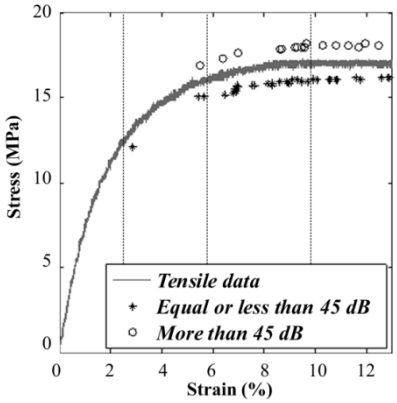

FIG. 8 STRESS/STRAIN CURVE AND AE DAMAGE BURSTS ACCORDING TO AMPLITUDE FOR PURE LLDPE.

Pure Matrix (0 wt% Fiber): KSOM Damage Mode Classification

Based on the key knowledge that a material exhibits phases related to damage mechanisms, in real life applications, it is important to reach a maximum reliability in dealing with damage mode evaluations. As plastic has very high damping characteristics, the amplitude is strongly dependent on the event location with respect to the sensor position. Consequently, it is important to evaluate not only the burst maximum amplitude but also its shape. The number of counts, the duration and the amplitude are important burst shape indicators.

In this section, KSOM is used to increase the discrimination accuracy by using additional burst parameters. KSOM is an unsupervised artificial neural network method that uses the principle of soft-learning. In this method, the neurons adjacent to the winner are weighted through a neighborhood function. All of the data relationships in the input are kept in the output because the algorithm processes information in a manner similar to that of the human brain. In spite of these advantages, results must be corroborated with previous knowledge to ensure that the artificial

network is analyzing data properly.

If the results corroborate well with previous knowledge, the result is a topological map referring to the damage modes. The results of the algorithm analyses are documented in the amplitude histogram of Fig. 9a. The graph includes two overlapping groups. These results are in agreement with the study presented in the previous section, confirming the validity of the current results.

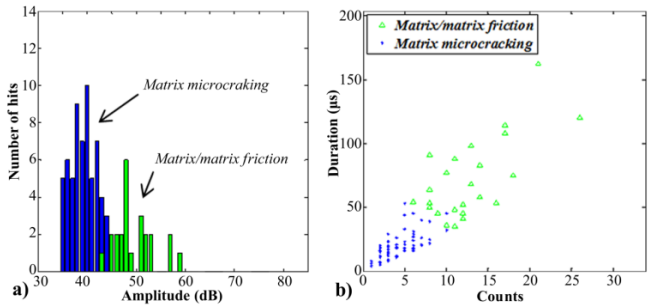

FIG. 9(a) AMPLITUDE HISTOGRAM SUCCESSFULLY DISCRIMINATED BY KSOM FOR PURE LLDPE; (b) COUNTS VERSUS DURATION ACCORDING TO KSOM.

The burst shape information for duration versus counts is documented in Fig. 9b. As expected, the two clusters with overlapping non-linear borders, which are similar to those found in the previous analysis, are good indicators that the discrimination is appropriate. The resulting AS of the matrix microcracking has a characteristic count number of up to 15 and a duration of up to 50 µs while the matrix/matrix friction has a minimum AS of 10 counts and a 25 µs duration.

Biocomposites: Pre-analysis of Damage Mode Classification

In this section, we study the failure mechanisms of the biocomposites. The amplitude distributions for specimens with 10 wt% and 30 wt% birch fiber are displayed in Fig. 10. In the first step, the mode boundaries found for the pure matrix specimens are used in the biocomposite histogram. This implies that mode I and II are already defined, in accordance with the first section (for a pure matrix).

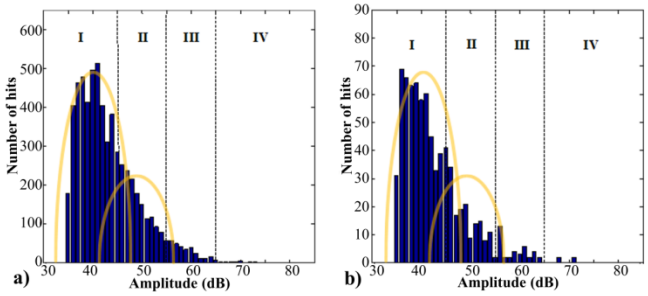

FIG. 10 AMPLITUDE HISTOGRAMS FOR BIOCOMPOSITES: (a) 10 WT% AND (b) 30 WT% FIBER.

The interpretation of the amplitude histograms starts from 55 dB. A discontinuity in shape is observed at 65 dB in both graphs. This suggests the existence of a boundary between the third and fourth modes, with the third group centered at 60 dB. The appearance of a decreasing slope is due to the overlap near 55 dB with mode II and the lack of overlap with mode IV. This last mode would have fewer bursts.

The literature suggests that groups III and IV represent decohesion and matrix/fiber friction, respectively. No bursts were observed from 85 dB to 100 dB, i.e., in the fiber breakage amplitude range; thus, mode V is inexistent due to the short fiber length (mean length: 0.489 mm ± 0.016 mm).

Biocomposites: KSOM Damage Mode Classification

In this section, the KSOM neural network is successfully applied for mode discrimination. The results of amplitude histograms for 10 wt% and 30 wt% are documented in Fig. 11. We denote four overlapping groups with limits close to those previously set in Fig. 10. Thus, the result from KSOM is in good agreement with the other data.

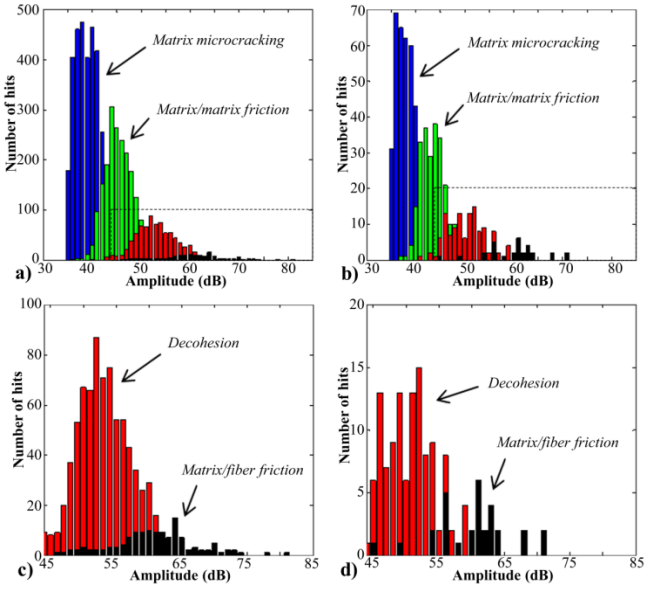

FIG. 11 AMPLITUDE HISTOGRAM SUCCESSFULLY DISCRIMINATED BY KSOM FOR BIOCOMPOSITES: (a) 10 WT% AND (b) 30 WT%. THE RESULTS OF DECOHESION AND MATRIX/FIBER FRICTION ONLY: (c) 10 WT% AND (d) 30 WT%.

For a better visualization, only the decohesion and matrix/fiber friction are documented in Fig. 11c and 11d. The substantial decohesion shown in the histograms reveals a poor matrix/fiber interface. For the 30 wt% specimen, the occurrence of final breakage with low strain contributed to the lower number of bursts recorded. The burst duration versus number of counts is shown in Fig. 12a for the 10 wt% specimen

and in Fig. 12b for the 30 wt% specimen.

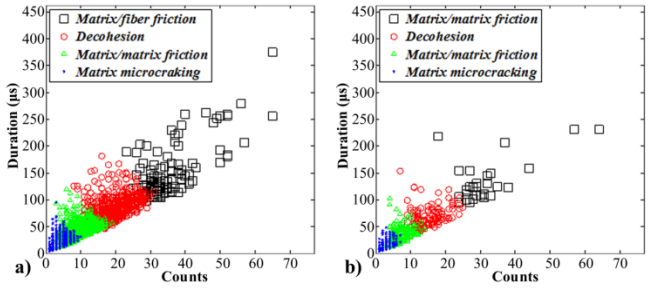

FIG. 12 COUNTS VERSUS DURATION ACCORDING TO THE MODES FOR BIOCOMPOSITES: (a) 10 WT% AND (b) 30 WT% FIBER.

The AS for the damage modes of the biocomposites was successfully discriminated. The multiparameter neural network analysis resulted in four clusters. The borders exhibited some overlapping, but there are still clear domains. As found before, the results were independent of the fiber weight used.

These results are summarized in Table 3. In this table, the AS of each damage mechanism is presented. The amplitude values are comparable to values found in the literature, but they are reinforced by two other parameters: the duration and the number of counts. This additional information allows for a consideration of the fuzziness in the AS that characterizes each damage mechanism. The results of this table can be useful for advanced mode recognition algorithms.

TABLE 3 SUMMARY OF DAMAGE AS.

Damage mode	Matrix micro-cracking	Matrix/ matrix friction	Decohesion	Matrix/ fiber friction
Amplitude (dB)	35-45	40-55	45-60	55-85
Duration (μs)	1-80	20-120	50-200	100-600
Counts	1-10	8-20	16-35	30-120

AE Failure Analysis Correlated to Mechanical Behavior

Once the AS is defined, the quantitative mode participation in specimen degradation can be assessed. We use the damage participation ratio (R_{ij}) proposed by Gong et al. which is defined as follows:

$$R_{ij} = \frac{(number\ \ of\ \ burts)_{ij}}{total\ \ number\ \ of\ \ burst} = \frac{m_{ij}}{m_R} \qquad (2)$$

"i" refers to the different modes of damage, "j" to the different load levels, and "m_R" to the total number of bursts at failure. With this definition, it is possible to observe the participation of each damage mechanism as a function of the material residual strain, as shown in Fig. 13.

Fig. 13 is a useful graph because it permits a comparison of the viscoelasticity with measured AE damage. For the 10 wt% specimen, a significant AE damage was observed only at 2.7% of the residual strain, after five cycles, suggesting that the initial increase in variable D (Fig. 3b) may be related to viscoelastic behavior. At this point, the mechanism of matrix/matrix friction contributed 3.19% of the damage. Decohesion and microcracking accounted for similar proportions, 2.41% and 2.40%, respectively. Matrix/fiber friction was the least damaging mode, which accounted for 1.33%, resulting in a total of 9.93% of the measured specimen damage.

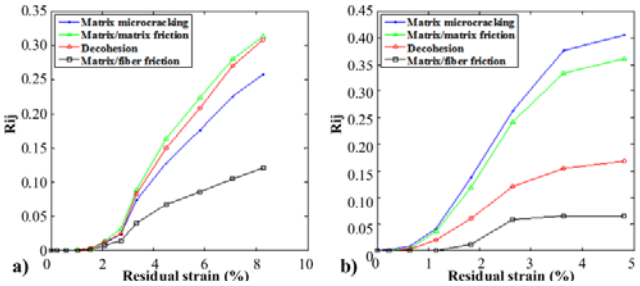

FIG. 13 EVOLUTION OF EACH DAMAGE MECHANISM FOR (a) 10 WT% AND (b) 30 WT% SPECIMENS

It is interesting to correlate the AE analysis with the mechanical behavior. As documented in Fig. 3a, the matrix and fiber of the material uncoupled starting from 4.2% of residual strain. We can see in Fig. 13a that in this cycle of uncoupling a substantial amount of AE activity occurred. At this point, decohesion contributed for 14% of material damage, causing 50% of total damage.

In the final failure, matrix/matrix friction was responsible for 31.42%, decohesion for 30.83%, matrix microcracking for 25.67% and matrix/fiber friction for 12.09%. Interestingly, as the biocomposite approached the final failure, the matrix microcracking accounted for less of the damage; instead, the matrix/matrix friction and decohesion were the dominating mechanisms.

In the case of the 30 wt% specimen, the first considerable damage occurred at 1.2% of the residual strain, after three cycles. At this stage, matrix microcracking accounted for 4.13% of the damage, matrix/matrix friction for 3.56% and decohesion for 2.02%. Matrix/fiber friction had not yet damaged the material, and the total measured damage was 9.71%.

Subsequently, the contribution of each damage mechanism in the final failure was: matrix microcracking, 40.53%; matrix/matrix friction, 36.13%; decohesion, 16.86%; and matrix/fiber friction, 6.48% of the total damage. It is interesting to note the low level of decohesion that occurred, even without a coupling

agent. This can be in part attributed to the lower level of stress on the interface matrix/fiber before the final failure occurs.

Scanning Electron Microscopy

To corroborate these results, the fractures were analyzed by SEM. Fig. 14a shows the fractured face of the 10 wt% specimen. A high amount of fiber decohesion led to many voids in the matrix. Furthermore, the high level of friction with the fibers (hard material) led to the surface aspect of a twisted matrix (soft material).

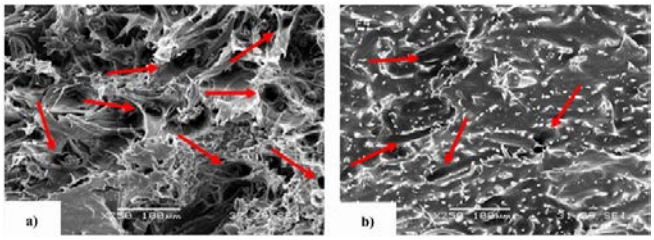

FIG. 14 FRACTURED FACE OF 10 WT% (A) AND 30 WT% (B) SPECIMENS: RED ARROWS INDICATE FIBERS THAT HAVE PULLED OUT.

The fractured face micrograph of the 30 wt% specimen (Fig. 14b) shows fewer fiber voids and a much less damaged matrix surface. As demonstrated by damage mode participation analysis, a lower level of decohesion and, subsequently, less matrix/fiber friction contributed to this surface condition, thus corroborating our results.

Conclusions

In this work, a biocomposite material was developed by mixing paper industry natural fibers (birch) and a thermoplastic matrix (LLDPE) at various fiber weights. Monotonic and load-unload tensile strength tests were conducted to measure the mechanical properties of the materials. An improvement in the elastic modulus and the ultimate strength was obtained for higher fiber weights. The manufacturing protocol used in this work demonstrates excellent measurement reproducibility with a low standard deviation.

AE instrumentation was used to assess the damage in the material along with a mechanical analysis of the stiffness drop. The evolution of the biocomposite behavior in four phases was documented using the AE energy. Exclusive damage modes (i.e., decohesion and matrix/fiber friction) increased the energy measured in the material degradation of the biocomposites. However, a participation analysis is only possible if a clear method of defining the AS is elaborated.

For this reason, in the first step only, general conclusions were drawn from the amplitude histogram for the pure matrix. Then, an artificial neural network using the KSOM was utilized, taking into account burst shape information on the counts and duration. The results corroborated the previous analysis, but misclassification was avoided to some extent.

This methodology was extended to biocomposites, which led to an AS classification for advanced algorithms with fuzzy boundaries. The participation of each mode in the final failure was finally evaluated. The results indicate that fiber content plays a primary role in biocomposite failure. This finding was supported by scanning electron microscopy (SEM) micrographs of the fractured face. With these encouraging results, it may be useful to study the degradation until failure of other forms of biocomposites, such as composites with both a matrix and a fiber from ecological sources.

ACKNOWLEDGEMENT

Lignocellulosic Materials Research Centre, Trois-Rivières (Canada).

REFERENCES

Barsoum, Fady F., Suleman, Jamil, Korcak, Andrej, and Hill, Eric.V. K. "Acoustic Emission Monitoring and Fatigue Life Prediction in Axially Loaded Notched Steel Specimens." Journal of acoustic emission 27 (2009): 40-63.

Bera, Moumita, Alagirusamy, R., and Das, Apurba. "A Study on Interfacial Properties of Jute-Pp Composites." Journal of Reinforced Plastics and Composites 29, no. 20 (2010): 3155-61.

Berthelot, Jean-Marie, and Rhazi, J. "Different Types of Amplitude Distributions in Composite Materials." Journal of Reinforced Plastics and Composites 7, no. 4 (1988): 302-20.

Bodig, Jozsef, and Jayne, B. A. "Mechanics of Wood and Wood Composites. Van Nostran-Reinhold Co." Inc., New York (1982).

Bravo, Alencar, Toubal, Lotfi, Koffi, Demagna, Erchiqui, Fouad, and Kokta, Bohuslav V. "Suivi par emission acoustique du Comportement et de l'endommagement d'un composite à matrice thermoplastique renforcée par des fibres de bouleau." RIED 2012 1 (2012): 4.

Czigány, Tibor. "Special Manufacturing and Characteristics

of Basalt Fiber Reinforced Hybrid Polypropylene Composites: Mechanical Properties and Acoustic Emission Study." Composites science and technology 66, no. 16 (2006): 3210-20.

El Mahi, Abderrahim, Ben Salem, Imen, Assarar, Mustapha, Berbaoui, Rachid, Poilane, Chritophe, and El Guerjouma, Rachid. "Analyse par émission acoustique de l'endommagement des matériaux éco-composites." Paper presented at the 10ème Congrès Français d'Acoustique, 2010.

Elouaer, Abdelmonem, Aboura, Zoheir, Ayad, Rezak, Sabhi, Hamid, and Benzeggagh, Malk. "Suivi de l'endommagement en fatigue des composites à base de fibres végétales = Monitoring of Fatigue Damage in Composites Based Fiber Plant." Paper presented at the 16èmes Journées Nationales sur les Composites (2009).

G'Sell, Christian. "Plasticité et endommagement des polymères structuraux." L'Actualité chimique, no. 3 (2002): 40-43.

Godin, Nathalie, Huguet, S., Gaertner, R., and Salmon, L. "Clustering of Acoustic Emission Signals Collected During Tensile Tests on Unidirectional Glass/Polyester Composite Using Supervised and Unsupervised Classifiers." NDT & E International 37, no. 4 (2004): 253-64.

Gong, Xiao-Lu, Laksimi, A., and Benzeggagh, M. L. "Nouvelle approche de l'émission acoustique et son application à l'identification des mécanismes d'endommagement dans les matériaux composites." Revue des composites et des Matériaux Composites Avancées 8, no. 1 (1998): 7-23.

Gu, Ruijun, Kokta, Bohuslav V., Michalkova, D., Dimzoski, B., Fortelny, I., Slouf, M., and Krulis, Z. "Characteristics of Wood-Plastic Composites Reinforced with Organo-Nanoclays." Journal of Reinforced Plastics and Composites 29, no. 24 (2010): 3566-86.

ISO 527-2. Determination of Tensile Properties - Part 2: Test Conditions for Moulding and Extrusion Plastics. Geneva: International Organization for Standardization, 1994.

ISO 527-4. Determination of Tensile Properties - Part 4: Test Conditions for Isotropic and Orthotropic Fibre-Reinforced Plastic Composites. Vol. 527, Geneva: International Organization for Standardization, 1997.

Jemielniak, Krzysztof. "Some Aspects of Acoustic Emission Signal Pre-Processing." Journal of Materials Processing Technology 109, no. 3 (2001): 242-47.

Kaiser, Josef. "Erkenntnisse Und Folgerungen Aus Der Messung Von Geräuschen Bei Zugbeanspruchung Von Metallischen Werkstoffen." Arch. Eisenhüttenwes 24, no. 1-2 (1953): 43-45.

Khan, Mubarak A., Masudul Hassan, M., and Drzal, Lawrence T. "Effect of 2-Hydroxyethyl Methacrylate (Hema) on the Mechanical and Thermal Properties of Jute-Polycarbonate Composite." Composites Part A: Applied Science and Manufacturing 36, no. 1 (2005): 71-81.

Kotsikos, George, Evans, J. T., Gibson, A. G., and Hale, J. "Use of Acoustic Emission to Characterize Corrosion Fatigue Damage Accumulation in Glass Fiber Reinforced Polyester Laminates." Polymer composites 20, no. 5 (1999): 689-96.

Lafia-Araga, Ruth A., Hassan, Aziz, Yahya, R., Rahman, Normasmira A., Hornsby, Peter R., and Heidarian, J. "Thermal and Mechanical Properties of Treated and Untreated Red Balau (Shorea Dipterocarpaceae)/Ldpe Composites." Journal of Reinforced Plastics and Composites 31, no. 4 (2012): 215-24.

Laksimi, Adbelouahed, Benmedakhene, S., and Bounouas, L. "Monitoring Acoustic Emission During Tensile Loading of Thermoplastic Composites Materials." Paper presented at the Proceeding of ICCM, 1999.

Lee, Seung G., Choi, Sung-Seen, Park, Won H., and Cho, Donghwan. "Characterization of Surface Modified Flax Fibers and Their Biocomposites with Phb." Paper presented at the Macromolecular Symposia, 2003.

Little, Elbert J. "Checklist of United States Trees (Native and Naturalized)." Agriculture Handbook, UK Department of Agriculture, no. 541 (1979).

Mark, Richard E. "Cell Wall Mechanics of Tracheids." Cell wall mechanics of tracheids. (1967).

Mehan, R. L., and Mullin, J. V. "Analysis of Composite Failure Mechanisms Using Acoustic Emissions." Journal of Composite Materials 5, no. 2 (1971): 266-69.

Meraghni, Fodil, and Benzeggagh, M. L. "Micromechanical Modelling of Matrix Degradation in Randomly Oriented Discontinuous-Fibre Composites." Composites science

and technology 55, no. 2 (1995): 171-86.

Miller, Ron K., and McIntire, P. "Nondestructive Testing Handbook. Vol. 5: Acoustic Emission Testing." American Society for Nondestructive Testing, 1987 (1987): 603.

Nourbakhsh, Amir, Ashori, Alireza, and Kouhpayehzadeh, Mojgan. "Giant Milkweed (Calotropis Persica) Fibers—a Potential Reinforcement Agent for Thermoplastics Composites." Journal of Reinforced Plastics and Composites 28, no. 17 (2009): 2143-49.

Nourbakhsh, Amir, Kokta, Bouhuslav V., Ashori, Alireza, and Jahan-Latibari, Ahmad "Effect of a Novel Coupling Agent, Polybutadiene Isocyanate, on Mechanical Properties of Wood-Fiber Polypropylene Composites." Journal of Reinforced Plastics and Composites 27, no. 16-17 (2008): 1679-87.

Physical Acoustics Corporation. PCI-2 Based AE System User's Manual. Princeton, NJ: Physical Acoustics Corporation, 2007.

Pollock, Adrian. "Acoustic Emission-2: Acoustic Emission Amplitudes." Non-destructive testing 6, no. 5 (1973): 264-69.

Raj, R. G., Kokta, Bohuslav V., Maldas, D., and Daneault, C. "Use of Wood Fibers in Thermoplastics. Vii. The Effect of Coupling Agents in Polyethylene–Wood Fiber Composites." Journal of applied polymer science 37, no. 4 (1989): 1089-103.

Santulli, Carlo. "A Biomimetic Approach to the Production of Sustainable Structural Composites Using Plant Fibres." Biologically inspired textiles, Woodhead Publishing (2008).

Toubal, Lotfi, Lorrain, B., Karama, M., and Marlot, D. "Composite Carbone/Époxyde: Suivi Par Émission Acoustique Et Caméra Infrarouge D'un Essai De Fatigue." Contrôles-Essais-Mesures 17 (2006): 26-28.

Vary, Alex. "Acousto-Ultrasonics - Retrospective Exhortation with Bibliography." Materials Evaluation 49, no. 5 (1991).